Designing an Agent-Based Model for Pericyte-to-Myofibroblast Transition in Lung Injury

Technical Report
Presented to the Faculty of the
School of Engineering and Applied Science
University of Virginia, Charlottesville, Virginia

By

Claire Hung, Undergraduate Department of Biomedical Engineering
Anahita H. Sharma, Undergraduate Department of Biomedical Engineering
Julie Leonard-Duke, Graduate Department of Biomedical Engineering
Riley T. Hannan, Ph.D., Department of Pathology
Shayn M. Peirce-Cottler, Ph.D., Department of Biomedical Engineering

Word Count: 3,462
Number of Figures: 6
Number of Tables: 1
Number of Equations: 5
Number of Supplements: 1
Number of References: 24

Advisor Approval: _____ Date: _____

Shayn M. Peirce-Cottler, Ph.D., UVA Department of Biomedical Engineering

Designing an Agent-Based Model for Pericyte-to-Myofibroblast Transition in Lung Injury

Claire Hung[a,*], Anahita H. Sharma[a,*], Julie Leonard-Duke[a], Riley T. Hannan, Ph.D.[b], Shayn M. Peirce-Cottler, Ph.D.[a,1]

[a] Department of Biomedical Engineering, University of Virginia
[b] Department of Pathology, University of Virginia
[1] Correspondence: S.M.P
Email: shayn@virginia.edu
Address: PO Box 800759, Health System, Charlottesville, VA 22908
Phone: 434-243-5795
* These authors contributed equally to this work

Abstract

Idiopathic pulmonary fibrosis (IPF) is a lethal lung disease with unknown cause and cure. The lack of understanding regarding the disease's pathophysiology and presence of ineffective treatments results in the high mortality of IPF. Previously, impeding the transition of pericytes into myofibroblasts, cells responsible for fibrotic lesions and tissue stiffening, was found to be a strategy for mitigating kidney fibrosis. Given lung pericytes are significant sources of myofibroblasts, we applied these findings to the pericyte-to-myofibroblast transition resulting from lung injury. Considering the time-efficient and cost-effective advantages of computational methods and the ability of such models to integrate key signaling pathways responsible for pericyte differentiation, we developed a two-dimensional agent-based model (ABM) to recapitulate the crucial signaling molecules and pericyte behaviors implicated in pulmonary fibrosis. The designed model can mimic the responses of pericytes, including migration, apoptosis, and differentiation, to transforming growth factor β (TGF-β), platelet-derived growth factor (PDGF), vascular endothelial growth factor (VEGF), and Thy-1 based on assigned rules. Sensitivity analysis was performed to assess the effect of cytokine perturbation on final myofibroblast count and extracellular matrix (ECM) stiffness after one-week and two-week simulations. Among all the signaling molecules, TGF-β exhibited the highest sensitivity coefficients for both myofibroblast number and ECM stiffness after one and two weeks. Higher TGF-β expression is associated with increased myofibroblast counts. However, downregulation of PDGF increased the ECM stiffness and lower VEGF concentrations reduced ECM stiffness after 1 week, contrary to the *in vivo* and *in vitro* findings. Furthermore, contrary to expectations, experiments showed a negative correlation between the initial number of active pericytes and average ECM stiffness. Therefore, we suggest future research focus on downregulating TGF-β and VEGF concentrations to most effectively decrease tissue stiffening associated with IPF progression.

Keywords: pericyte, myofibroblast, fibrosis, agent-based model

Introduction

IPF is a chronic, progressive pneumonia characterized by excessive ECM deposition within the pulmonary interstitium[1,2]. Owing to the poor prognosis, the median survival rate of patients with IPF is approximately 3-5 years post-diagnosis[3]. This highly lethal disease has affected more than 500,000 individuals in the United States and results in a $2 billion financial burden annually[1,4]. Myofibroblasts are the main players contributing to wound healing and tissue remodeling. Dysregulated ECM secretion by myofibroblasts in lung injury results in excessive ECM deposition within the lung interstitium, tissue thickening and stiffening, and ultimately respiratory failure[5]. The accumulation of myofibroblasts and ECM proteins, which gives rise to fibroblastic foci, is regarded as the hallmark of IPF and is directly correlated to disease severity and

mortality[6,7]. However, the pathophysiology of IPF has not yet been fully understood, contributing to the limited efficacy of the current standard of care for IPF. Two existing FDA-approved IPF medications, Nintedanib and Pirfenidone, can impede disease progression, but fail to reduce the mortality of the disease, implying an urgent need for novel IPF therapeutics.

Pericytes, the mural cells wrapping the capillaries, are critical to the formation of new vessels[8]. The coverage of pericytes around endothelial cells is crucial to structurally stabilize the capillary wall, regulate the capillary diameter, and maintain vascular homeostasis[8]. In addition to the roles pericytes play in microcirculation, pericytes are also one of the most significant sources of myofibroblast progenitors. In lung fibrosis, pericytes are capable of transitioning into myofibroblasts, detaching from the capillary walls, and migrating to the interstitial regions of the lung. A previous study has found that halting the pericyte-to-myofibroblast transition can ameliorate renal fibrosis in type I diabetic nephropathy[9]. In addition, current FDA-approved IPF drugs downregulate multiple cytokines and tyrosine kinases involved in microvascular remodeling, which includes TGF-β, PDGF receptors, and VEGF receptors[4,6]. These works together suggest the significance of microvascular alteration in the progression of pulmonary fibrosis, thereby increasing the potentiality of vascular components as novel therapeutic targets for IPF.

Due to the high cost of research and complexity of clinical trials, designing a computational model can provide researchers and developers of IPF treatments the ability to study their hypotheses in a controlled, time-efficient, and cost-effective manner prior to conducting *in vitro* and *in vivo* experiments. With regard to tissue fibrosis outside of the lungs, a mathematical model on renal interstitial fibrosis originating from tubulointerstitial inflammation was developed[10]. This model approximated the densely packed tubules and blood vessels in renal tissue as a rectangle. Spatial and temporal densities of macrophages, which contribute to inflammation; fibroblasts; ECM; and cytokines such as PDGF, matrix metalloproteinase (MMP), and TGF-β were represented through a set of partial differential equations (PDEs) with periodic boundary conditions. However, models such as this one, which rely heavily on ordinary differential equations (ODEs) and partial PDEs, prevent discovery of the emergent phenomena and incorporation of multiple scales of biological processes,

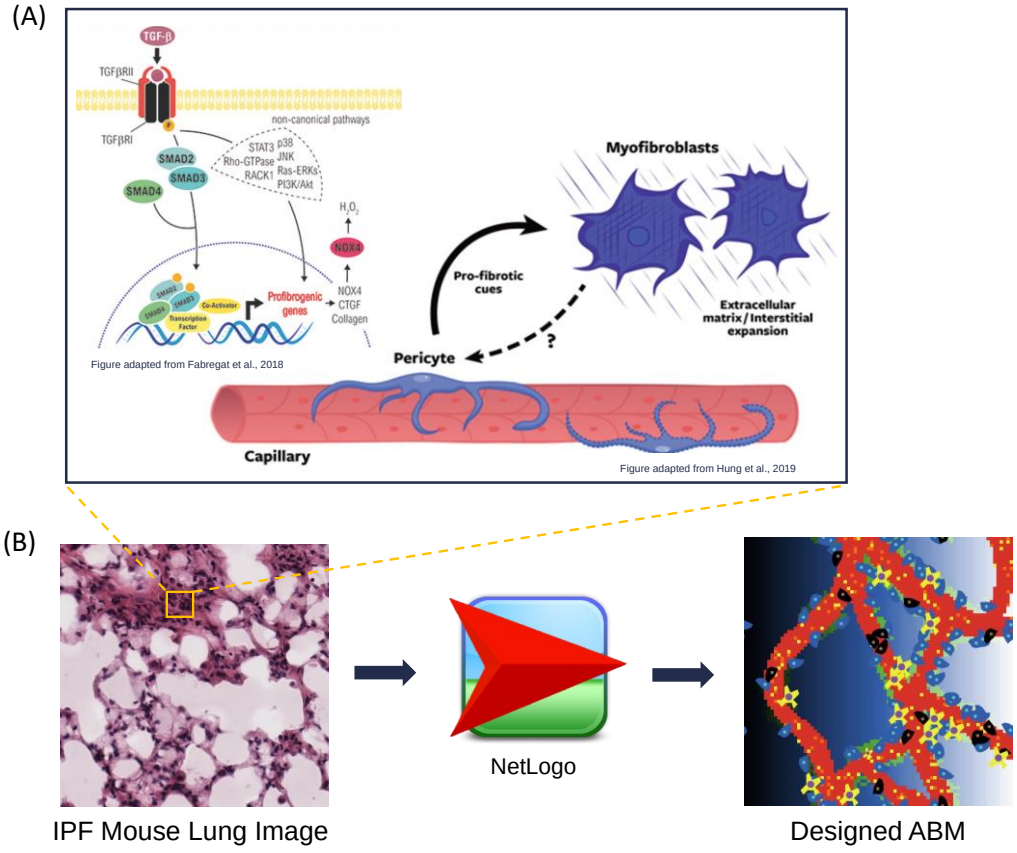

Fig. 1. Design idea of the proposed model. (A) Signaling pathways involved in IPF: Figure adapted from Fabregat et al., 2018 that depicts how the presence of extracellular TGF-β can induce the expression of profibrogenic factors such as collagen. Figure adapted from Hung et al., 2019 depicts morphological changes of pericyte upon encountering profibrogenic cues. (B) Overview of the use of NetLogo in representing histology images computationally. Histology images obtained from past lab paper studying pulmonary microvasculature.

both of which are crucial when attempting to draw tissue-wide conclusions from the data[11].

ABMs, on the other hand, enforce a set of "rules", which are represented as logic-based conditions or differential equations, on individual "agents." The ability to incorporate spatial considerations with an intuitive modeling paradigm suggests that ABMs are better suited for translational biology than other types of computational models, especially given that unveiled emergent phenomena are sometimes counterintuitive to what is expected[12]. This was exemplified in a hybridized physics and agent-based model used to recapitulate IPF progression[13]. In this model, 2D lung tissue was modeled using a hexagonal network of linear springs. The spaces in the hexagons represented alveoli and fibroblasts were located at the network's nodes. Changes in stiffness due to increased ECM deposition were mimicked by increasing the spring constant of the hexagons where the agents were activated by existing stiff ECM.

However, existing models still do not account for environmental cues that activate the pericyte-to-myofibroblast transition and its impact on ECM remodeling. The development of a multiscale computational model that investigates the influence of various biochemical cues on the differentiation of pericytes into myofibroblasts following lung injury would enable comparison with experimental data for prediction validation and provide a platform for identifying and validating new therapeutic interventions for IPF. Therefore, through combining the previous *in vitro* and *in vivo* findings, we aim to develop a two-dimensional ABM that can simulate the responses of pericytes, including proliferation, migration, and transition, to diverse signaling pathways (Figure 1). In addition to incorporating the essential biochemical stimuli – TGF-β, VEGF, and PDGF – Thy-1, a membrane protein responsible for mechanosensing by interacting with αvβ3 integrin, will be used to simulate mechanotransduction in our model[14]. Through this resulting model, the sensitivity of the pericyte-to-myofibroblast transition to various chemical

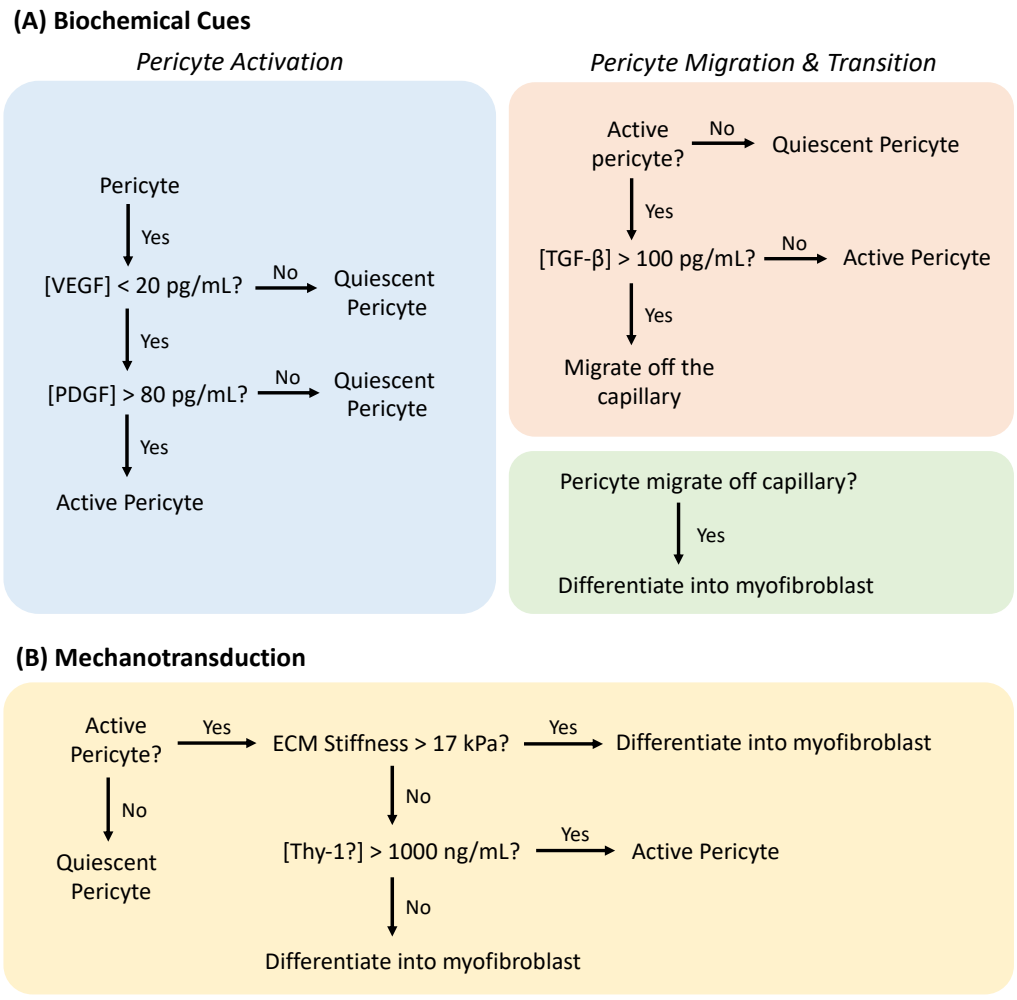

Fig. 2. Rule flowchart for pericyte behaviors in the developed ABM. (A) The blue box depicts the responses of pericytes to VEGF and PDGF. Pericytes are defined as "active" if the concentration of VEGF is lower than 20 pg/mL and the concentration of PDGF is higher than 80 pg/mL. Active pericytes will migrate off vessels and have the potential to differentiate into myofibroblasts. The orange and green boxes describe the pericyte behaviors in response to TGF-β stimulation. If an active pericyte is in the region with TGF-β concentration higher than 100 pg/mL, it will migrate off the capillary and transition into a myofibroblast. (B) Pericytes sensing the ECM stiffness > 17 kPa will differentiate into myofibroblasts. However, Thy-1 with a concentration lower than 1000 ng/mL would also cause pericyte-to-myofibroblast transition even if the ECM stiffness is lower than 17 kPa.

and mechanical cues can be uncovered as a means of improving the understanding of IPF and accelerating the development of therapeutics for this disease.

Results

Rule Flowchart Defining Pericyte Behaviors

In this ruleset, we depicted the cellular behaviors that are implemented in the designed model, including pericyte activation, pericyte migration off the blood vessels, and pericyte transition into myofibroblasts (Figure 2A). The rules for pericyte responses to molecule signaling are condition-based and are determined by simple yes-or-no questions. We defined "active" pericytes as the pericytes that can differentiate into myofibroblasts, while "inactive" pericytes are pericytes that remain quiescent even in the presence of biochemical and mechanical stimuli. The activation state of pericytes is determined by the concentrations of both VEGF and PDGF signaling molecules. Given that VEGF contributes to the stability of capillaries and PDGF can lead to pericyte detachment from the vessels, we posited that pericytes present in regions with a VEGF concentration less than 20 pg/mL and a PDGF concentration higher than 80 pg/mL are defined as "active" pericytes[15,16]. The pericytes not meeting this criterion are deemed as "inactive", or quiescent, pericytes. To model the pericyte response to biochemical cues, we chose to develop a rule for TGF-β due to the essential role TGF-β plays as a profibrotic factor in the progression of pulmonary fibrosis. If the agent is confirmed as an active pericyte and stimulated by a patch where the TGF-β concentration is higher than 100 pg/mL, the pericyte will then differentiate into a myofibroblast[10]. These stimulated pericytes, or myofibroblasts in this case, will then have the potential to detach from the capillary and migrate toward the lung interstitium. The baseline values of VEGF, PDGF, and TGF-β used to form these rules can be found in Table 1.

The mechanosensing of ECM stiffness that induces the lung pericyte transition is incorporated through the interaction of the Thy-1 and αvβ3 integrins (Figure 2B). If the active pericytes sense a patch with an ECM stiffness larger than 17 kPa, the typical stiffness of fibrotic pulmonary tissue that is approximately 30 times higher than the Young's modulus of healthy lung tissue, they will undergo differentiation into myofibroblasts[17]. On the other hand, if the ECM stiffness is lower than 17 kPa, Thy-1 would be the determinant factor on the fate of activated pericytes. Since the lack of Thy-1 in injured lungs will result in increased αv integrin activation regardless of the ECM stiffness and exacerbate the tissue scarring, the activated pericytes without the presence of a Thy-1 concentration exceeding 1000 ng/mL will transition into myofibroblasts even when the tissue has a stiffness lower than 17 kPa[18]. The baseline concentration of Thy-1 and the stiffness of fibrotic lung tissue can be found in Table 1. The above-mentioned chemical and mechanical cues simultaneously regulate the fate of pericytes in the developed model.

Table 1. Parameters for designed ABM. Parameters in this table include those used to recapitulate chemical and morphological characteristics of native lung tissue in humans. Due to the limited availability of information regarding IPF tissue in humans, parameters derived from other human organ systems and bleomycin-induced mouse models were also used.

Parameter	Value	Reference
VEGF Concentration	20 pg/mL	Murray et al., 2017
Thy-1 Concentration	1000 ng/mL	Tan et al., 2019
PDGF Concentration	80 pg/mL	Prasad et al., 2014
TGF-β Concentration	100 pg/mL	Hao et al., 2014
Pericyte Diameter	6-10 μm	Hartmann et al., 2015 & Grant et al., 2019
Pericyte Migration Rate	11.875 μm/hr	Tigges et al., 2013
Myofibroblast Diameter	12.14 μm	Baum et al., 2011
Capillary Diameter	7 μm	Short et al., 1996
Fibrotic ECM stiffness	17 kPa	Wells et al., 2013
Time for 1 tick	15 minutes	N/A
Total simulation time	1-2 weeks	N/A

2D ABM Simulating Phenotypic Switch of Lung Pericytes

The lung microenvironment, including the alveolar and vascular architectures, of fibrotic lungs was designed using the historical immunofluorescence murine lung images collected in the Peirce-Cottler lab. Blood vessels with tortuous features are represented by the red-colored patches, which make up the background of the model (Figure 3). The yellow and orange patches denote areas where there is a higher concentration of VEGF and PDGF, respectively. Per the rules mentioned above, these cytokines allow the pericytes to become activated or remain as inactive. The gradient of TGF-β stuck in the lung ECM was represented by the blue-to-white color gradient in the model background. Additionally, we used green patches to denote TGF-β secreted by active pericytes with the potential to transition into myofibroblasts. Thy-1 expression and behaviors elicited through mechanosensing were achieved by creating a patch-variable for ECM stiffness that is increased upon pericyte differentiation and a mechanotransduction function that implements the rules above (Figure 2B). A reporter function was included to report the average ECM stiffness in patches with a stiffness greater than that of healthy tissue (0.5 kPa). We leveraged

this reporter function to graph ECM stiffness in our model's main console.

Pericytes, the primary agents of our proposed model, have been incorporated into the model as turtles so they are able to travel around the model and respond to changes in their surroundings. To mimic the coverage of pericytes around endothelial cells in the microvasculature, we made the diameters of the pericytes approximately equal to the diameters of capillaries, which is 7 μm[19]. The pericytes possess the ability to undergo apoptosis, migrate along and off the vessels, and differentiate into myofibroblasts through the interactions with incorporated cytokine signaling pathways. The black, blue, and yellow cells stand for quiescent pericytes, active pericytes, and myofibroblasts, respectively.

Given the diversity of the units for the parameters (Table 1), it was crucial that we appropriately time-scale and dimensionally-scale the parameters of our model to match the duration of each tick. A tick in NetLogo is an iterator that aids in continuously running the model's functions. For the purposes of our model, each tick represented a change in time. This enabled us to make periodic conclusions about the pericyte-to-myofibroblast transition over varying periods of time. As our initial simulations approximated at most a two-week timeline, we decided to have each tick represent 15-minute increments. In the model's console, we enabled users to choose the total number of pericytes, including both the active and inactive ones, to better simulate the desired conditions. The dimensions for the cross-sectional area, which will impact the scaling of migration rate parameters, for example, can also be controlled manually. The concentrations of VEGF, PDGF, Thy-1, and TGF-β are adjustable as well using sliders. An output plot in our console visually displays active/quiescent pericyte and myofibroblast counts, and another plot that

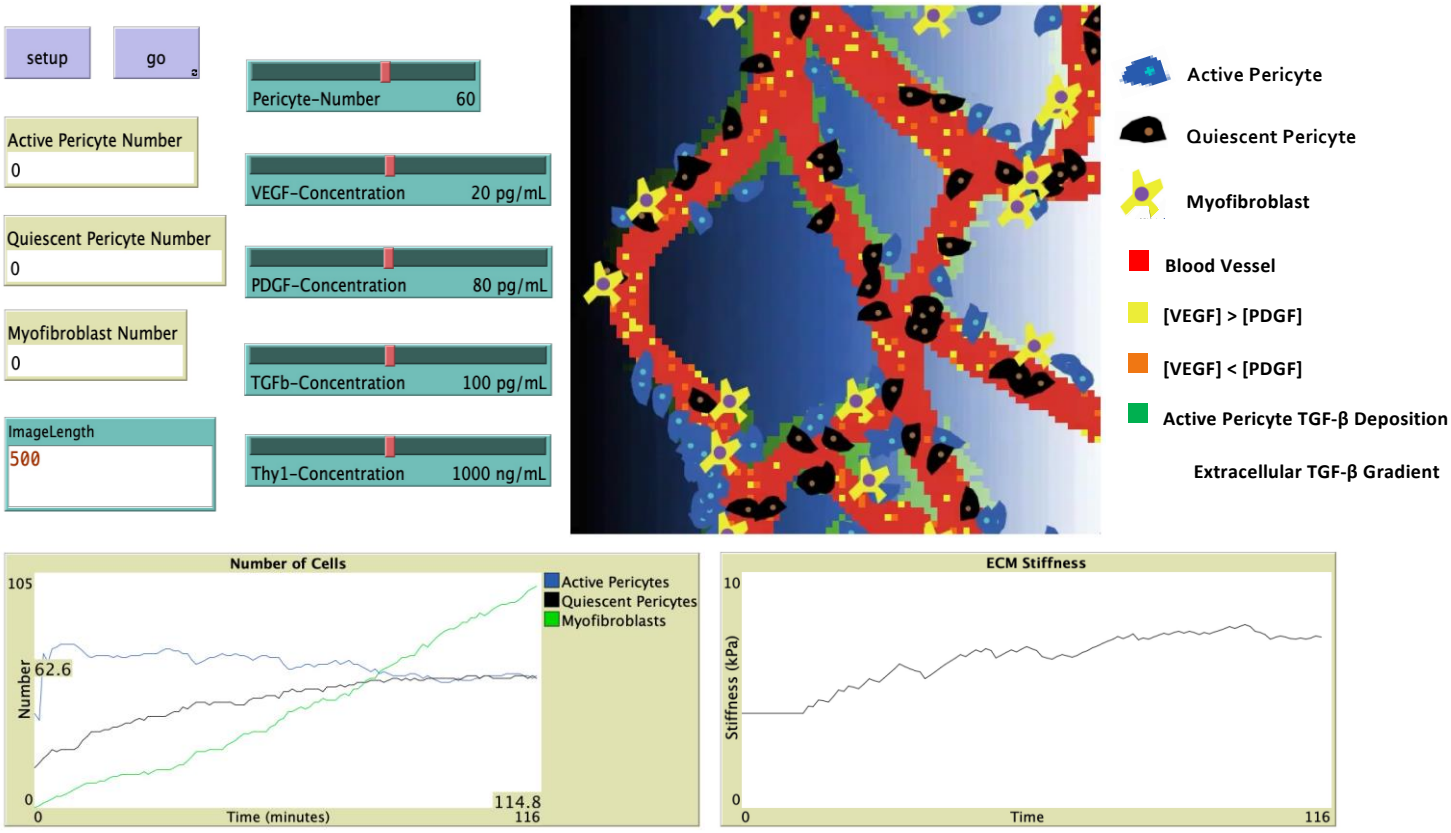

Fig. 3. ABM console as designed in NetLogo. The console of the ABM, as designed in NetLogo, contains a series of buttons, monitors, inputs, sliders, and plots that a user may utilize to study the influence of mechanical and chemical cues on the progression of IPF. The buttons *setup* and *go* execute the setup and go functions of the model (described in the Agent-Based Model Development and Optimization section). Monitors display counts of active pericytes, quiescent pericytes, and myofibroblasts currently in the model. The input field for ImageLength enables the user to specify the size of the tissue they want to examine. Sliders enable users to specify the initial active pericyte count (Pericyte-Number) and cytokine concentrations that control agent behavior. Plots graph the output values for counts of agents over time and average ECM stiffness over time.

manifests the ECM stiffness provides a real-time readout at each time point.

Number of Pericytes and ECM Stiffness

Our initial experiments focused on studying how the number of active pericytes present at the start of the simulations altered the average ECM stiffness of the tissue at the end of the simulation. Figure 4 depicts how changes in initial active pericyte number altered the average ECM stiffness observed at the end of a one week long experiment. Per prior studies, it was expected that as the initial active pericyte count increased, the ECM stiffness would increase as well as there would be a higher number of pericytes present capable of differentiating into myofibroblasts. However, as can be seen in Figure 4, a negative association between the two variables was observed, counter to what was expected.

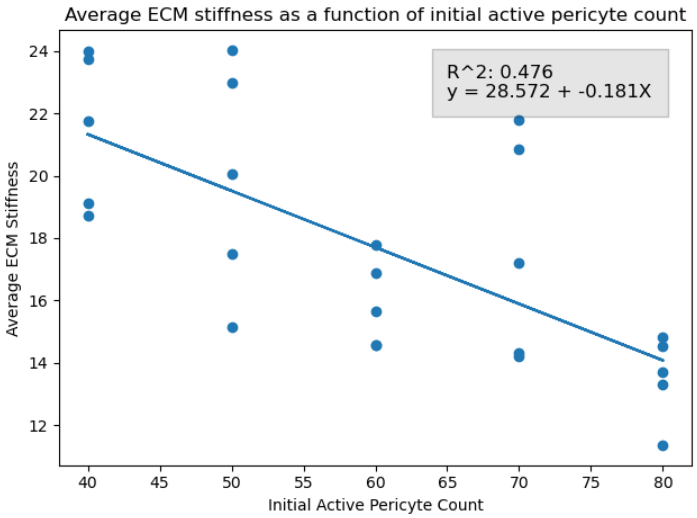

Fig. 4. Changes in ECM stiffness as a function of the number of active pericytes in the model initially. As the number of active pericytes present in the model initially increases, the average final ECM stiffness of the simulated tissue decreases. The experiment was run with n = 5 for each parameter value.

Impacts of Parameter Perturbation on System Outcomes

To assess the effects of the perturbation of signaling molecules on model outputs, we performed sensitivity analysis for changes in TGF-β, Thy-1, PDGF, and VEGF to study their influence on final myofibroblast count and ECM stiffness. Based on the original, baseline values of the model (Table 1), where [TGF-β] = 100 pg/mL, [Thy-1] = 1000 ng/mL, [PDGF] = 80 pg/mL, and [VEGF] = 20 pg/mL, 10%, 20%, 40%, 60%, 80%, and two-fold (i.e., 100%) increases and decreases in cytokine concentrations were tested for the analyses. As 1 week and 2 weeks are common timeframes for evaluating the pericyte-to-myofibroblast transition caused by lung injury in bleomycin-induced murine models, we performed the sensitivity analyses on each group after 1-week and 2-week simulations, which are equivalent to 672 and 1,344 ticks, respectively, in the model. Owing to the relationship between pericyte number and ECM stiffness (Figure 4), 60 was used as the initial pericyte number to avoid the bias resulting from extremely low or high counts. In this model, we defined 30% of the total initial number of pericytes as "quiescent" pericytes while the remaining as "active" pericytes. Consequently, 60 counts of total initial pericytes correspond to 42 "active" pericytes and 18 "quiescent" pericytes at time zero. Each group was repeated 5 times and the mean values of 5 runs were used to calculate the sensitivity coefficients.

<u>Cytokine Concentration and Myofibroblast Count</u>

After a 1-week simulation, most conditions demonstrated that as the concentration of TGF-β increased, there was an increased number of myofibroblasts relative to baseline. Similarly, lower TGF-β expression was associated with lower myofibroblast count (Figure 5A). These findings are consistent with prior *in vivo* and *in vitro* findings. It is worth noting that the two highest sensitivity coefficients of TGF-β occurred when the concentration was changed to a 10% increase and decrease from baseline. These changes were notably also the highest sensitivity coefficients observed among all groups. A similar trend was seen with percent decreases of TGF-β concentration, which had higher sensitivities after 2 weeks. However, a significant increase in sensitivity, contrary to previous studies, was also found. Among all the signaling molecules, TGF-β exhibited the highest sensitivity coefficient across all concentrations at both 1-week and 2-week time points (Figure 5B). The sensitivity of PDGF is extremely low after one week, but it significantly increases after a two-week simulation. Higher Thy-1 expression reduces myofibroblast activation after 1 week, agreeing with the prior finding. Nevertheless, the increased Thy-1 concentrations correspond to enhanced myofibroblast counts after 2 weeks, which is contrary to what we expected. Although VEGF does not show a high sensitivity, the downregulation of VEGF correlates with increased myofibroblast presence after both 1-week and 2-week simulations, meeting our initial expectations.

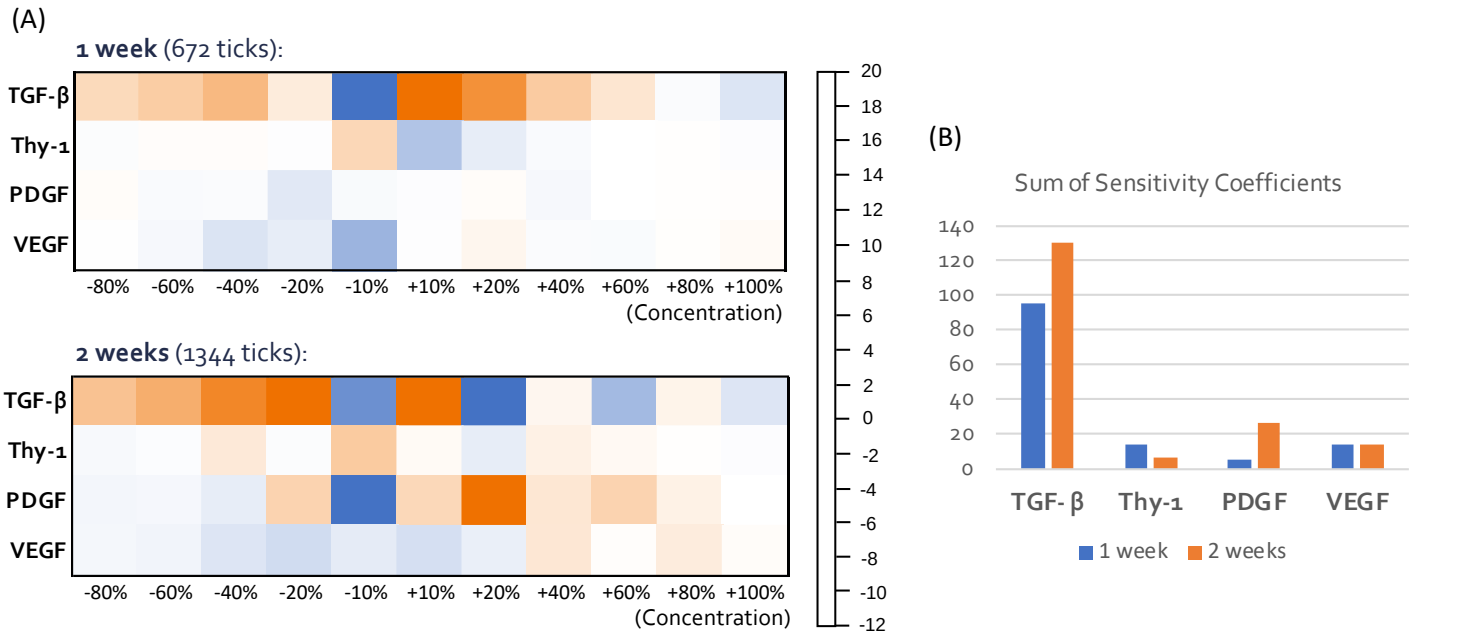

Fig. 5. Sensitivity analysis of simulated signaling molecules on myofibroblast count. (A) 10%, 20%, 40%, 60%, and 80% increase and decrease in the concentrations of signaling molecules were used to assess how cytokine perturbation affected the number of myofibroblasts. All groups were compared to [TGF-β] = 100 pg/mL, [Thy-1] = 1000 ng/mL, [PDGF] = 80 pg/mL, and [VEGF] = 20 pg/mL. Each color block represents the sensitivity coefficient calculated using Equation 4. The initial number of total pericytes and active pericytes was 60 and 42, respectively. n = 5 for all groups. The highest coefficients occur at ±10% and ± 20% for TGF-β and PDGF. (B) The absolute value of sensitivity coefficient at different concentrations was added to determine the molecule possessing the highest sensitivity on myofibroblast count. TGF-β showed the highest sensitivity among all groups while Thy-1 has the lowest after both 1 and 2 weeks.

Holistically, the highest sensitivity values were seen at minor perturbations of –10%, +10%, and +20% in both 1-week and 2-week simulations.

Cytokine Concentration and ECM Stiffness

Aside from the number of myofibroblasts, the increased tissue stiffness caused by ECM protein deposition is a vital feature of lung injury. Therefore, another set of sensitivity analysis on ECM stiffness was performed using the same initial conditions and comparison criteria as the analysis on myofibroblast count (Figure 6A). TGF-β exhibits the highest sensitivity holistically, which, however, is not as prominent as it was in the results regarding myofibroblast count (Figure 6B). It was also found that after 2 weeks, the sensitivity coefficients showed a significant increase following both a 10% decrease and increase in VEGF concentration. The downregulation of VEGF contributed to reduced ECM stiffness after both 1 week and 2 weeks. Nevertheless, the reduced ECM stiffness was also seen in the upregulation of VEGF after 2 weeks, which is contradictory to prior wet-lab studies. Overall, the sensitivity coefficients for both Thy-1 and PDGF are low within all concentration groups, suggesting the minimal effects of perturbations in Thy-1 and PDGF concentrations on pulmonary ECM stiffness. It is worth noting that compared to the scale bar of analysis on the number of myofibroblasts, the maximal and minimal values on the scale bar in the sensitivity analysis of ECM stiffness are two to three times lower, which implies the higher stability of ECM stiffness in response to cytokine concentration perturbations.

Discussion

The mortality of IPF has failed to be mitigated by existing FDA-approved therapeutics, thereby necessitating further study into the mechanisms through which IPF develops and progresses. Our project aimed to design a two-dimensional ABM that integrated the novel pericyte-to-myofibroblast transition, recently implicated in the progression of renal fibrosis, to elucidate its role in the progression of IPF. Specifically, we aimed to understand how pericytes involved in this transition pathway responded to diverse biochemical stimuli and mechanical cues, as assessed by myofibroblast counts and ECM stiffness. One-week and two-week simulations using this model aimed to mimic

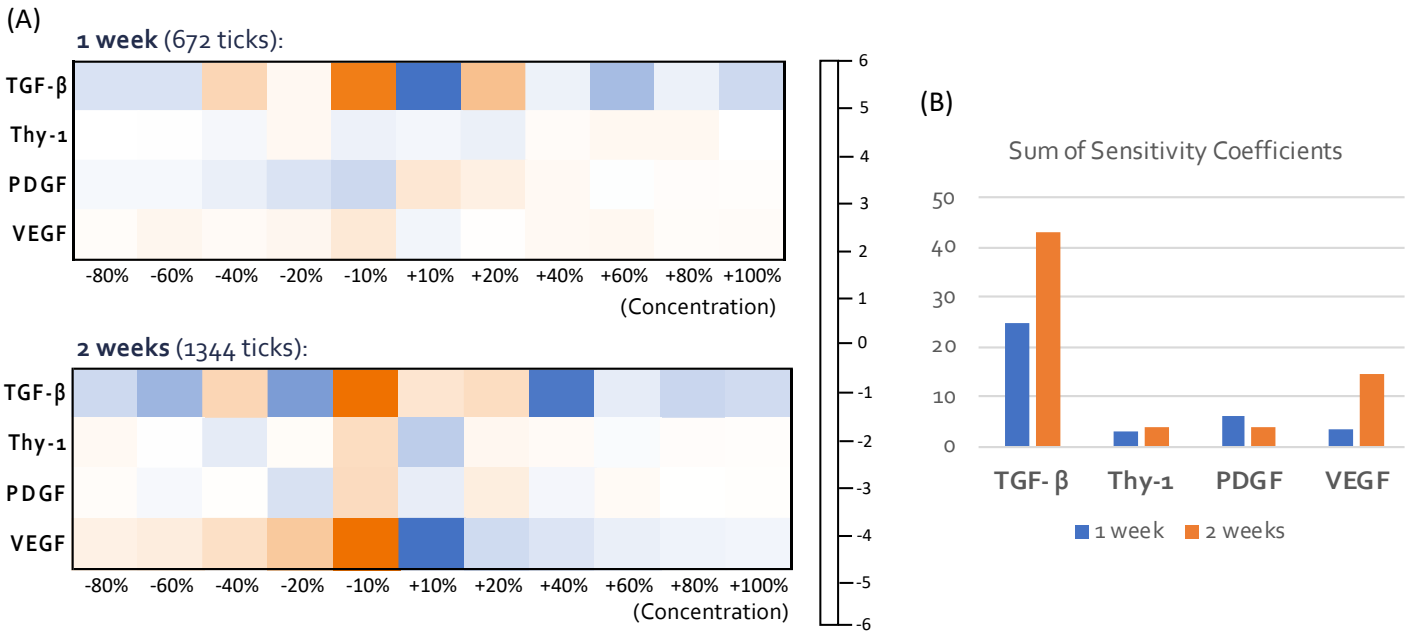

Fig. 6. Sensitivity analysis of simulated signaling molecules on ECM stiffness. (A) 10%, 20%, 40%, 60%, and 80% increase and decrease in the concentrations of signaling molecules were used to assess how cytokine concentrations perturb the stiffness of ECM. All groups were compared to [TGF-β] = 100 pg/mL, [Thy-1] = 1000 ng/mL, [PDGF] = 80 pg/mL, and [VEGF] = 20 pg/mL. Each color block represents the sensitivity coefficient calculated using Equation 4. The initial number of total pericytes and active pericytes was 60 and 42, respectively. n = 5 for all groups. The highest coefficients occur mostly at ±10% for TGF-β and VEGF. (B) The absolute value of sensitivity coefficient at different concentrations was added to determine the molecule possessing the highest sensitivity on ECM stiffness. TGF-β showed the highest sensitivity among all groups while Thy-1 has the lowest after both 1 and 2 weeks.

timeframes for *in vivo* experimentation performed on mice with bleomycin-induced lung injuries.

Firstly, it was found that there is a slight negative association between the initial active pericyte count in the tissue and eventual ECM stiffness, which was contrary to our expectations. The experiments completed using this model also suggested IPF progression, as represented by the final myofibroblast count and average ECM stiffness, is most sensitive to TGF-β signaling. As TGF-β concentration was decreased, a decrease in myofibroblast count and ECM stiffness was observed. Furthermore, as predicted, downregulation of VEGF correlated with increased myofibroblast presence, however contrary to expectations, simultaneously reduced ECM stiffness. Additionally, the role of PDGF on the pericyte-to-myofibroblast transition became increasingly important at longer time points, with the upregulation of PDGF increasing myofibroblast count and ECM stiffness after 2 weeks, as was expected. However, this linear relationship was not maintained as when PDGF was downregulated it increased ECM stiffness. Overall, the sensitivity of the model to PDGF and Thy-1 remained relatively low over the course of both one and two weeks, suggesting that these two cytokines had limited influence over the pericyte-to-myofibroblast transition pathway, and ultimately the progression of IPF. Therefore, our team suggests that future research on IPF and its treatments target the downregulation of TGF-β and VEGF to decrease ECM stiffness observed during fibrosis most effectively.

Overall, while there were aspects of our results that corroborated previously published studies regarding the impact pro-fibrotic cytokines had on the progression of fibrosis, there were findings, such as those associated with VEGF signaling and initial active pericyte count, that differed from our expectations. While these unexpected findings can be attributed to the study of emergent phenomena unique to ABMs, there are a series of future steps that can be taken to ensure the accuracy of these findings. Firstly, we recommend increasing the complexity of the behaviors associated with the various agent breeds. For example, our model did not enable myofibroblasts to migrate, however, it is known that myofibroblasts migrate to and are highly responsive to chemokines released at the site of injuries[20]. In addition, further optimizing the model's parameters such that they include values specific to human pulmonary tissue would increase the likeness of our model

to *in vivo* conditions. Thus, while this model aims to be a cost-effective platform for IPF research, it requires additional preliminary wet-lab experiments to be performed to enhance the accuracy of its behaviors. Furthermore, given that alveoli possess a three-dimensional (3D) structure, incorporating 3D features into the model can aid in further understanding patterns associated with tissue stiffening and myofibroblast localization.

Through such changes, we project this model can aid in identifying a potential target for treating IPF, and eventually serve as an *in silico* testing platform for evaluating the effectiveness of proposed IPF therapeutics. Given the user-friendly interface of NetLogo and its intent to be used by individuals of all ages and backgrounds, this model can be adapted by researchers of all specialties to include and test specific hypotheses. Thereby, reaching its goal of serving as a cost- and time-effective platform for IPF research.

Materials and Methods

Materials

The entirety of this project was completed on personal computers with NetLogo Version 6.2.0 installed. NetLogo is a free, open-source software that provides users with a programmable modeling environment to simulate natural and social phenomena[21]. Additionally, JupyterLab, launched using the free Individual Edition of Anaconda, was used as a means of pre-processing and manipulating the sensitivity analysis data in Python for downstream visualization.

Methods

Design Constraints and Assumptions

As this ABM is intended to serve as a preliminary testing platform for future *in vivo* and *in vitro* experimentation related to pulmonary fibrosis, our team aimed to simulate as accurately as possible the main features of native IPF lung tissue. However, we still had to make a series of assumptions regarding the various behaviors and environmental cues implemented in our model. Firstly, we assumed that all "active" pericytes differentiate directly into myofibroblasts. However, it is known that pericytes *in vivo* can differentiate into numerous other cell types, such as fibroblasts, myointimal cells, and vascular smooth muscle cells (VSMCs)[22]. This assumption enabled us to make direct conclusions about the influence changing cytokine parameters played on the pericyte-myofibroblast transition and alterations in ECM stiffness. Additionally, we assumed that "inactive" pericytes, in comparison to "active" pericytes which were agents activated by benchmarks for cytokine concentration and ECM stiffness, did not possess the ability to proliferate, migrate, or differentiate. Specifically, as we were interested in simulating one- and two-week timeframes, which are traditionally used for bleomycin-induced lung injury mice model experiments, the actions of these "inactive" pericytes were assumed to be largely insignificant, and thus omittable from our model.

With regards to the cytokine signaling pathways in our model, we assumed that the extracellular TGF-β concentration gradient was one-dimensional and at steady state. Per Fick's Second Law of Diffusion (Equation 1) under constant boundary conditions (Equation 2), the TGF-β concentration gradient was modeled by Equation 3 where *C(x)* represents the concentration along the horizontal axis of the ABM, which models lung tissue *L* μm in width. While the console of our model allows users to specify *L* by inputting an integer for ImageLength (Figure 3), we assumed C_1 = 100 ρg/mL and C_2 = 0 ρg/mL. The TGF-β concentration gradient can be visualized in our model as the blue-to-white color gradient in the background (Figure 3).

$$\frac{\partial C}{\partial t} = D\frac{\partial^2 C}{\partial x^2} \quad [1]$$

$$C(0) = C_1, \quad C(L) = C_2 \quad [2]$$

$$C(x) = \frac{C_2 - C_1}{L}x + C_1 \quad [3]$$

As it relates to mechanosensing and ECM stiffness, we assumed that there was a linear relationship between collagen secreted by the active pericytes and myofibroblasts and ECM stiffness. Within the model, one "unit" of collagen deposition following the migration of an active pericyte or myofibroblast on to a patch caused a 1 kPa increase in ECM stiffness at that patch.

Agent-Based Model Development and Optimization

To reiterate, the purpose of this ABM was to integrate biochemical cues, such as VEGF, PDGF, TGF-β, and Thy-1 signaling, with mechanical cues brought on by mechanotransduction to understand their impact on the pericyte-to-myofibroblast transition, and ultimately the stiffening of pulmonary tissue seen in IPF. The developed 2D ABM was designed using object-oriented programming in NetLogo. In NetLogo, there are two major classes of agents – turtles and patches. Turtles possess the ability to interact with the system based on a logic-based ruleset, while patches are pixels with fixed locations in the simulated environment that constitute the background and contain information regarding the local environment. To implement the various desired features into our model, we developed new breeds of turtles – Pericytes, Quipericytes, and Myofibroblasts to represent active pericytes, quiescent pericytes, and myofibroblasts, respectively. Each of these breeds contained a variety of variables, such as *migrate*, *mech_td*, and *thy-1*, which guided each breed's ability to migrate and respond to mechanotransduction depending on the breed's associated activation level. To represent the

extracellular TGF-β cytokine gradient, cellular cytokine deposition, and mechanotransduction, patches in the ABM contained unique variables for VEGF, PDGF, and TGF-β concentration, along with a patch-variable for stiffness. These patch variables were used to direct agent behavior per the flowchart depicted in Figure 2.

To mimic the tortuous structure of pulmonary microvasculature, prior histology images of healthy lung tissues were used to inform the design of a standard vessel image that accounted for alveolar space, as seen by the gaps between vessel structures, which are in red (Supplementary Figure 1). Within the *setup* function of the model, which is run prior to any simulation, the colors of the standard vessel image were imported such that patches in the corresponding locations of the model acquired the red color representing the vessel branches. The *setup* function also ran functions we developed related to setting up the extracellular TGF-β concentration gradient per Equations 1-3, randomly assigning VEGF and PDGF concentrations to patches along the vessel, establishing a baseline tissue stiffness of 0.5, and assigning *migrate* and *mech_td* to appropriate Boolean values of True or False for each agent breed.

Following the setup of the model, the *go* function was run with each tick (i.e. step of the model). For our simulations, each tick represented 15 minutes, as mentioned in Table 1. With each execution of the *go* function, other functions specific to each breed's behavior were run. Briefly, quiescent pericyte behaviors in the model were limited to apoptosis. Active pericyte behaviors included inactivation (to quiescent pericytes), proliferation, migration, differentiation, apoptosis, TGF-β deposition, and ECM stiffening. Finally, myofibroblast behaviors were limited to ECM stiffening, but at a level three times greater than that of active pericytes. Each of these behaviors is directed by the ruleset in Figure 2, which is regulated by cytokine signaling pathways and mechanotransduction sensing capabilities of these agents.

During the original iteration of the model, our team built the model with arbitrary values assigned to each of the relevant variables. However, after completing this first-generation model, we conducted an iterative literature review until we ultimately found all the parameters listed in Table 1 that best represented each included parameter. These optimized parameter values were implemented into the model by simply updating the values of variables representing these parameters. Furthermore, these optimized values served as baseline parameter values for sensitivity analyses that were performed later. Within our optimized model, we also added sliders that allowed users to specify cytokine concentrations relevant to regulating pericyte activation, migration, and differentiation status. This enables users to understand the emergent phenomena that results from cumulative changes in investigated cytokine concentrations.

To ensure that pericyte behaviors corresponded with the timelines *in vivo*, parameter values were time-scaled to the ticks and dimensionally scaled to the size of the model. For example, the migration rate of active pericytes was both time- and dimensionally-scaled using the metric 1 tick equals 15 minutes and the dimensional variable ImageLength. This ensured that pericytes did not travel further than expected per previously acquired histology images of lung tissue.

Sensitivity Analysis

Sensitivity analysis aims to measure how the model reacts to changes in parameters or other input values[23]. This procedure helps identify parameters with the strongest influence on model output, thereby indicating processes in the model that are the most important[24]. Furthermore, in cases where parameter values are uncertain, sensitivity analysis can help assess the importance of these uncertainties. However, in our study, we aimed to use sensitivity analysis as a means of understanding cytokine signaling pathways that had the most significant impact on myofibroblast count and ECM stiffness in lung tissue, such that these pathways can be investigated as targets for future IPF treatments.

To perform sensitivity analysis, our team used BehaviorSpace, an integrated software tool in NetLogo that allows users to perform experiments with their models. Within BehaviorSpace, we ran experiments altering the VEGF, PDGF, TGF-β, and Thy-1 parameter values at increments of 10% from their baseline values listed in Table 1. Parameter values ranged from an 80% decrease from their baseline value to a 100% increase from their baseline value. For example, when running experiments altering VEGF concentration, which has a baseline value of 20 ρg/mL, the variable *VEGF-Concentration* took on values from 4 ρg/mL to 40 ρg/mL at increments of 2 ρg/mL. The other cytokine concentration parameter values were maintained at baseline, as listed in Table 1. Meanwhile, ImageLength was set to 500 μm and Pericyte-Number was set to 60. Experiments collected data from the ECM stiffness variable, *ECM_Stiffness*, and counts for the three agent types – Pericytes, Quipericytes, and Myofibroblasts. These output values were saved, along with their corresponding input values, into a CSV file. For this study, one cytokine parameter was changed in each experiment in the manner mentioned above. Each experiment was run 5 times (i.e. n = 5) for 672 ticks or 1,344 ticks to mimic one-week or two-week *in vivo* mice experiments, respectively.

To analyze the relationship between active pericyte count and average ECM stiffness, a similar experimentation method as above was adopted. The active pericyte counting variable, *Pericyte-Number*, was changed by increments of 10 cells such that a range of 40 to 80 active pericytes was investigated while all other parameter values were maintained at baseline. The resulting output value, ECM stiffness, was graphed against the input values and a linear

regression was performed on the data. The coefficient of determination, R^2, was calculated for this linear regression model.

Data Analysis

Output CSV files generated from the BehaviorSpace experiments were analyzed in Python, launched through the JupyterNotebook application of Anaconda. Data from the CSV files were structured into table objects from the Tables class of the datascience package. Table manipulation enabled output reads at final timepoints of 672 or 1,344 ticks to be identified and then grouped by the value for the altered cytokine parameter. The grouped values were then averaged. Then, Equation 4 was applied to data columns containing the altered cytokine parameter and its associated average output values for ECM stiffness and myofibroblast count. In Equation 4, P_0 represents the baseline value for the parameter being changed, ΔP represents the change from baseline of the parameter being changed, Y_0 represents the output value associated with the baseline parameter condition, and ΔY represents the change in output value compared to Y_0. Positive values for sensitivity coefficients indicate a positive association between the input parameter and the output parameter (i.e. as the input value increased, so did the output value). Whereas, a negative sensitivity coefficient indicates a negative association between the input and output values (i.e. as the input value increased, the output value decreased, or vice versa). These sensitivity coefficients were used to generate heatmaps such as those seen in Figures 5 and 6.

$$S = \frac{\Delta Y}{\Delta P}\frac{P_0}{Y_0} \quad [4]$$

To determine the cytokine with the greatest impact over the studied output – myofibroblast count or ECM stiffness – Equation 5 was used. In this equation, n represents the various concentrations studied for each cytokine and S equals the associated sensitivity coefficients calculated for each parameter value. Higher values for I indicate a greater impact of the parameter on the output variable, and lower values for I indicate a lower influence of the parameter on the output value.

$$I = \sum |S_n| \quad [5]$$

End Matter

Author Contributions and Notes

C.H. and A.H.S. researched, designed, and developed the proposed ABM. S.M.P., J.L.D., and R.T.H advised the development of the proposed ABM. C.H. and A.H.S. also analyzed the data and wrote the paper.

The authors declare no conflict of interest.

Acknowledgments

We would like to thank Dr. Shayn M. Perice-Cottler, Julie Leonard-Duke, and Dr. Riley T. Hannan for their guidance and expertise during this project. We would also like to thank the University of Virginia Department of Biomedical Engineering and University of Virginia Department of Pathology for facilitating this project.

References

1. Spagnolo, P., Tonelli, R., Cocconcelli, E., Stefani, A. & Richeldi, L. Idiopathic pulmonary fibrosis: diagnostic pitfalls and therapeutic challenges. Multidiscip. Respir. Med. 7, 42 (2012).
2. Barratt, S. L., Creamer, A., Hayton, C. & Chaudhuri, N. Idiopathic Pulmonary Fibrosis (IPF): An Overview. J. Clin. Med. 7, 201 (2018).
3. Fernández Fabrellas, E., Peris Sánchez, R., Sabater Abad, C. & Juan Samper, G. Prognosis and Follow-Up of Idiopathic Pulmonary Fibrosis. Med. Sci. 6, (2018).
4. King, T. E. et al. Idiopathic pulmonary fibrosis: relationship between histopathologic features and mortality. Am. J. Respir. Crit. Care Med. 164, 1025–1032 (2001).
5. Hinz, B. et al. The Myofibroblast. Am. J. Pathol. 170, 1807–1816 (2007).
6. Wollin, L. et al. Mode of action of nintedanib in the treatment of idiopathic pulmonary fibrosis. Eur. Respir. J. 45, 1434–1445 (2015).
7. Moore, M. W. & Herzog, E. L. Regulation and Relevance of Myofibroblast Responses in Idiopathic Pulmonary Fibrosis. Curr. Pathobiol. Rep. 1, 199–208 (2013).
8. Barron, L., Gharib, S. A. & Duffield, J. S. Lung Pericytes and Resident Fibroblasts: Busy Multitaskers. Am. J. Pathol. 186, 2519–2531 (2016).
9. Chang, F.-C., Chou, Y.-H., Chen, Y.-T. & Lin, S.-L. Novel insights into pericyte-myofibroblast transition and therapeutic targets in renal fibrosis. J. Formos. Med. Assoc. Taiwan Yi Zhi 111, 589–598 (2012).
10. Hao, W., Rovin, B. H. & Friedman, A. Mathematical model of renal interstitial fibrosis. Proc. Natl. Acad. Sci. 111, 14193–14198 (2014).
11. Leonard-Duke, J. et al. Multi-scale models of lung fibrosis. Matrix Biol. 91–92, 35–50 (2020).
12. An, G., Mi, Q., Dutta-Moscato, J. & Vodovotz, Y. Agent-based models in translational systems biology. Wiley Interdiscip. Rev. Syst. Biol. Med. 1, 159–171 (2009).
13. Wellman, T. J., Mondoñedo, J. R., Davis, G. S., Bates, J. H. T. & Suki, B. Topographic distribution of idiopathic pulmonary fibrosis: a hybrid physics- and agent-based model. Physiol. Meas. 39, 064007 (2018).
14. Hagood, J. S. Thy-1 as an Integrator of Diverse Extracellular Signals. Front. Cell Dev. Biol. 7, (2019).
15. Murray, L. A. et al. Antifibrotic role of vascular endothelial growth factor in pulmonary fibrosis. JCI Insight 2, (2017).
16. Prasad, S., Hogaboam, C. M. & Jarai, G. Deficient repair response of IPF fibroblasts in a co-culture model of epithelial injury and repair. Fibrogenesis Tissue Repair 7, 7 (2014).
17. Wells, R. G. Tissue mechanics and fibrosis. Biochim. Biophys. Acta BBA - Mol. Basis Dis. 1832, 884–890 (2013).

18. Tan, C. et al. Soluble Thy-1 reverses lung fibrosis via its integrin-binding motif. JCI Insight 4, (2019).
19. Short, A. C. et al. Pulmonary capillary diameters and recruitment characteristics in subpleural and interior networks. J. Appl. Physiol. 80, 1568–1573 (1996).
20. Baum, J. & Duffy, H. S. Fibroblasts and Myofibroblasts: What are we talking about? J. Cardiovasc. Pharmacol. 57, 376–379 (2011).
21. NetLogo User Manual (version 6.2). https://ccl.northwestern.edu/netlogo/faq.html.
22. Rowley, J. E. & Johnson, J. R. Pericytes in Chronic Lung Disease. Int. Arch. Allergy Immunol. 164, 178–188 (2014).
23. Combined use of local and ANOVA-based global sensitivity analyses for the investigation of a stochastic dynamic model: Application to the case study of an individual-based model of a fish population. Ecol. Model. 193, 479–491 (2006).
24. Thiele, J. C., Kurth, W. & Grimm, V. Facilitating Parameter Estimation and Sensitivity Analysis of Agent-Based Models: A Cookbook Using NetLogo and R. J. Artif. Soc. Soc. Simul. 17, 11 (2014).

Supplementary Figures

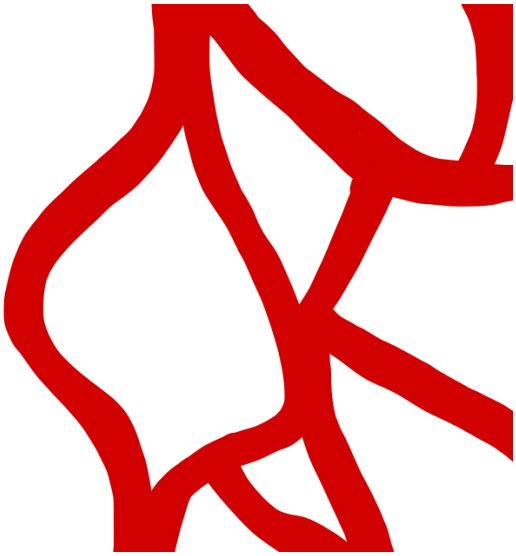

Supplementary Figure 1. Standard vessel image used for ABM development. This image was used to create vessel structures in the ABM. This image was illustrated by leveraging previously published histology images of healthy lung tissue to recapitulate a section of microvasculature in lung tissue. The white gaps between vessel branches represent alveoli.